Towards perfectly linearly polarized x-rays

Kai S. Schulze,[1,2,3,*] Benjamin Grabiger,[1,2,3] Robert Loetzsch,[1,2] Berit Marx-Glowna,[1,3] Annika T. Schmitt,[1,2] Alejandro Laso Garcia,[4] Willi Hippler,[2] Lingen Huang,[4] Felix Karbstein,[1,3,5] Zuzana Konôpková,[6] Hans-Peter Schlenvoigt,[4] Jan-Patrick Schwinkendorf,[6] Cornelius Strohm,[6,7] Toma Toncian,[4,6] Ingo Uschmann,[1,2] Hans-Christian Wille,[7] Ulf Zastrau,[6] Ralf Röhlsberger,[1,2,3,7] Thomas Stöhlker,[1,2,3] Thomas E. Cowan,[4,8] and Gerhard G. Paulus[1,2]

[1]*Helmholtz-Institut Jena, Fröbelstieg 3, 07743 Jena, Germany*
[2]*Institut für Optik und Quantenelektronik, Friedrich-Schiller-Universität Jena, Max-Wien-Platz 1, 07743 Jena, Germany*
[3]*GSI Helmholtzzentrum für Schwerionenforschung, Planckstraße 1, 64291 Darmstadt, Germany*
[4]*Helmholtz-Zentrum Dresden-Rossendorf, Institute of Radiation Physics, Bautzner Landstraße 400, 01328 Dresden, Germany*
[5]*Theoretisch-Physikalisches Institut, Abbe Center of Photonics, Friedrich-Schiller-Universität Jena, Max-Wien-Platz 1, 07743 Jena, Germany*
[6]*European XFEL GmbH, Holzkoppel 4, 22869 Schenefeld, Germany*
[7]*Deutsches Elektronen-Synchrotron DESY, Notkestraße 85, 22607 Hamburg, Germany*
[8]*Technische Universität Dresden, 01062 Dresden, Germany*

(Received 27 May 2021; revised 26 November 2021; accepted 11 February 2022; published 23 March 2022)

In recent years, high-precision x-ray polarimeters have become a key method for the investigation of fundamental physical questions from solid-state physics to quantum optics. Here, we report on the verification of a polarization purity of better than 8×10^{-11} at an x-ray free-electron laser, which implies a suppression of the incoming photons to the noise level in the crossed polarizer setting. This purity provides exceptional sensitivity to tiny polarization changes and offers intriguing perspectives for fundamental tests of quantum electrodynamics.

DOI: 10.1103/PhysRevResearch.4.013220

I. INTRODUCTION

Polarization is a fundamental property of electromagnetic fields. Its control and measurement are of importance in many fields of modern optics from communication [1,2], ellipsometry [3], and remote sensing [4] to quantum cryptography [5–7] and quantum optics [8]. In the x-ray range, polarization plays a pivotal role as well. It provides insights into the structure of materials via x-ray dichroism [9,10] and enables the detection of quantum optical phenomena [11–13]. The advent of x-ray free-electron lasers (XFELs) has paved new avenues in x-ray physics, in particular, with polarized x rays. These will allow, for example, the investigation of the structure of the magnetic fields evolving in solid density plasma [14] as well as the detection of a fundamental quantum physical phenomenon, namely, vacuum birefringence [15–20]. As already predicted in the early days of quantum electrodynamics [21], even the empty space can change the polarization of light in the presence of a strong electromagnetic field [15,16]. As a consequence, linearly polarized light becomes elliptically polarized after passing through the vacuum. The resulting ellipticity scales linearly with the photon energy of the probe beam, and, thus, the intensity ratio of the elliptic axes scales with the square. Therefore, x rays instead of visible light are expedient to increase the signal significantly. But even with x rays, the expected intensity ratio is below 10^{-11} for the fields generated by multiple 100-TW lasers, which are currently available at XFELs [17–20]. The effect will even be small for the extreme fields provided by the 100-PW laser system, which is currently under construction in Shanghai [22,23].

To reach the highest sensitivity to polarization changes as well as a perfect control of quantum states in quantum optics, the experimental realization of a perfect polarization state is an aspired goal. However, there will always be a small portion of light polarized in the orthogonal polarization state to the desired one and unpolarized parts. For linear polarization, a measure for the deviation from perfect polarization is the polarization purity P. It is defined as the intensity ratio of two orthogonal polarization states and would be zero in the case of perfect polarization [24].

Based on previous work on x-ray polarizers [25–29], there has been tremendous progress in their development in recent years, especially through the development of channel-cut crystals [30–34]. Whereas the principle is rather simple, the design of these polarizers is not. Channel-cut polarizers facilitate multiple consecutive reflections with a scattering angle $2\Theta_B$ of 90° inside a channel, which is cut into a monolithic crystal. At this angle, the polarization component parallel to the scattering plane is strongly attenuated. However, the crystalline structure influences the degree of polarization. The choice of crystal material, its cut, and method of surface treatment are, therefore, crucial for high polarization

*kai.sven.schulze@uni-jena.de

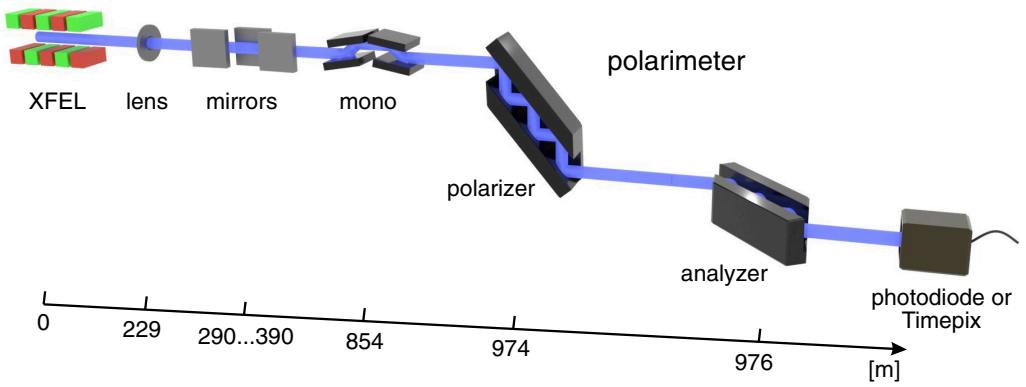

FIG. 1. Scheme of the experimental setup used to create perfect linear polarization. The XFEL radiation with a photon energy of 6.457 keV was collimated to a high degree by a beryllium lens, followed by mirrors, which guided the beam to the experiment. A high-heat load monochromator (mono) selected and stabilized the photon energy and reduced the heat load on the polarizer. The polarimeter consisted of two so-called channel-cut crystals made from silicon. Each of the crystals supported six consecutive reflections with a scattering angle of 90°. The analyzer crystal could be rotated around the beam to analyze the created polarization state.

purities [30,31]. Using highly optimized channel cuts, we could already demonstrate a polarization purity of 2.4×10^{-10} [31].

Imperative for high purities is the proper azimuthal orientation of the lattice planes to circumvent polarization-changing multiple-wave diffraction [31,32]. If crystal structure and orientation are highly symmetric, multiple-wave diffraction will be suppressed effectively. Therefore, perfect polarization can only be achieved with low-order reflections at cubic crystals, for instance, the 400 reflection of silicon or diamond [32].

To achieve ultimate performance of an optical instrument, the entire setup and not only parts have to be scrutinized. Indeed, a recent theoretical work predicts that not only the polarizers determine the polarization purity, but also the properties of the light source, in particular, its divergence [32]. For perfect polarizers, the achievable polarization purity is limited to

$$P \approx \sigma_{\mathrm{h}}^2 + \sigma_{\mathrm{v}}^2, \tag{1}$$

where σ_{h} and σ_{v} are the root-mean-square divergences in the horizontal and vertical directions, respectively [32]. At third-generation synchrotron radiation sources, the horizontal divergence σ_{h} of the undulator radiation is usually on the order of 10 μrad. The polarization purity is, therefore, limited to about 10^{-10} [33]. In contrast, XFELs provide laserlike x-ray beams with much higher brilliance. Their radiation can be collimated to a high degree by lenses to reach divergences of less than 1 μrad [35].

In this paper, we report on the realization of an unprecedentedly pure linear polarization state realized at one of the most brilliant x-ray sources.

II. EXPERIMENT AT THE EUROPEAN XFEL

The experiment was performed at the High Energy Density (HED) instrument of the European XFEL in Germany. Figure 1 shows a sketch of the experimental setup. The XFEL was operated in self-amplified spontaneous emission (SASE) mode with a repetition rate of ten pulses per second and a mean pulse energy of about 1.4 mJ. The x-ray beam was collimated to a high degree by a beryllium lens located 229 m behind the source. At 171 and 710 m behind the lens, the beam size was measured to determine the divergence. The full width at half maximum was 591 (898) and 244 (898 μm) in the horizontal (vertical) direction, respectively. These values correspond to a root-mean-square divergence of $\sigma_{\mathrm{h}} = 273$ nrad in the horizontal and a negligible divergence in the vertical direction, which, in turn, is suitable to achieve a theoretical limit for the polarization purity of 7×10^{-14} according to Eq. (1). We estimate the error of this measurement to be 10%.

Crucial for the realization of high polarization purities are the setting and stability of the photon energy. For this reason, we used a monochromator with the added benefit of less heat load on the polarizer. In contrast to mirrors, x-ray diffraction at crystals only occurs if scattering angle and photon energy fulfill the Bragg condition. Therefore, the monochromator as well as the XFEL had to be precisely set to a photon energy corresponding to the scattering angle $2\Theta_{\mathrm{B}} = 90^\circ$ within our channel-cut crystals. In this experiment where the silicon 400 Bragg reflection was chosen, a photon energy close to 6.457 keV was required. We verified the setting of the absolute photon energy using a method similar to that of Bond [36] with an accuracy of 1 eV. For that reason, the incident x rays were reflected at a silicon crystal using the same Bragg reflection as for the polarizers in two different settings: reflecting the x rays upwards and downwards. If the angular positions of the crystal for these two settings differ by 90°, the wavelength is set correctly. The 1-eV uncertainty corresponds theoretical to a maximum deterioration of the polarization purity by 5×10^{-7} for one reflection and 1×10^{-33} for the chosen polarizers with six consecutive reflections.

The core of the experimental setup, the polarimeter, consisted of two optimized channel-cut crystals, each supporting six consecutive reflections. The first crystal acts as a polarizer to strongly enhance the polarization purity of the XFEL radiation. The second one, the analyzer, is required to analyze the resulting polarization state. It can be rotated around the beam axis from the setting where the scattering planes of both polarizers are parallel to the perpendicular one. The latter is

also known as the crossed polarizer setting. Both crystals had an optimized azimuthal orientation in such a way that the projection of the incident beam on the lattice planes is along the ⟨0 1 1⟩ crystallographic direction [32]. The inner surfaces of the channels were treated by a combination of lapping and etching to minimize distortions of the wavefront. Since the distance between the two channel walls is only 6 mm, the surfaces were lapped by hand. This allowed also to treat them with a random motion.

Since we expected an intensity variation of, at least, ten orders of magnitude when the polarization analyzer is turned from the parallel to the crossed polarizer setting, we used two different detectors to measure the intensity. For most of the analyzer angles, the photocurrent of a photodiode was used as a measure of the number of incident photons in a given time interval. The photodiode was calibrated at the Physikalisch-Technische Bundesanstalt. This calibration allows the conversion from the measured photocurrent to the radiation power and, consequently, to the number of incident photons. The photocurrent was measured with a Keithley amperemeter, which was triggered to the XFEL's repetition rate of 10 Hz. Close to the analyzer angle of 90°, an energy- and space-resolving TIMEPIX detector [37] was used for single-photon counting. The energy resolution allows distinguishing multiple-photon hits and background radiation. The acquisition time window of the TIMEPIX detector was set to 10 s. At each angular position, ten exposures were acquired resulting in an integration over 1000 XFEL pulses. We used the time-over-threshold mode to get information about the deposited energy in each pixel. Faulty pixels were excluded from the analysis. A cluster analysis within a region-of-interest allowed the reconstruction of events that spread over several pixels. The sum of the pixel values within these clusters allows the reconstruction of one or multiple photon events and, thus, the calculation of count rates. We checked with different measurements that the count rates received with both detectors are equal within the statistical uncertainty. Together, both detectors covered a dynamic range of more than 11 orders of magnitude.

III. RESULTS

As expected, the intensity behind the polarimeter dropped dramatically by several orders of magnitude during the variation of the analyzer angle from the parallel ($\eta = 0°$) to the crossed setting ($\eta = 90°$) as shown in Fig. 2(a). The data points represent the integrals of the respective rocking curves, two of which are shown exemplarily as insets. Because of the integration over a finite number of XFEL pulses and the stochastic nature of SASE radiation, there are small deviations from the theoretical $\cos^2(\eta)$ behavior. The insets (b) and (c) show the count rate when the analyzer's incident angle was rocked at $\eta = 0°$ and $\eta = 90°$, respectively. In the latter, no significant signal above background is observable, although each data point was integrated over 1000 XFEL pulses. More precisely, there are 11 counts in the angular range where a signal is expected (marked region) and 11 counts outside. The latter corresponds to a background of 0.016 cps (upper 95% confidence level) based on Poisson statistics. Because of the low number of events, a reliable determination

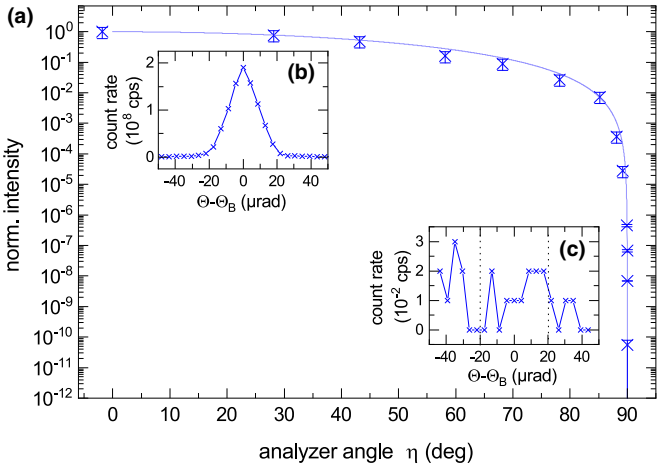

FIG. 2. (a) Dependence of the intensity behind the polarimeter when the analyzer was rotated from the parallel polarizer setting at 0° to the crossed polarizer setting at 90°. The data points are the integrals of the rocking curve normalized to the value at 0°. The solid line represents the $\cos^2$ behavior expected for perfect polarizers. Insets (b) and (c) show the count rate when the analyzer crystal is rocked in the parallel and the crossed setting, respectively. In the latter, no rocking curve above the noise level can be detected. The dotted lines mark the region in which the curve is expected.

of the proportion of scattered radiation and detector noise to the background is not possible. It must be noted that there were just 6×10^7 photons per pulse (6×10^8 photons per second at 10-Hz repetition) behind the polarizer because of the mismatch of the SASE bandwidth and the energy acceptance of the crystals, the reflectivity of the crystals, and the absorption in air.

Figure 3 shows the throughput of the polarimeter upon the variation of the analyzer angle η in a region close to $\eta = 90°$ for a fixed incident angle corresponding at the maximum of the rocking curve. The measurements were performed with an energy- and space-resolving TIMEPIX detector accumulating 1000 XFEL pulses. For selected analyzer angles, also the spatial distribution of the intensity is shown. This measurement underpins that no photon above background (represented as the gray-shaded area) could be detected at an analyzer angle η of exactly 90°. Consequently, only an upper boundary of the polarization purity can be given. The ratio of the background to the number of photons behind parallel polarizers gives an upper bound of the polarization purity of 6.5×10^{-11} (95% confidence level) if no remaining signal photons in the crossed polarizer setting are assumed. If one assumes signal photons hidden in the background, an upper bound can be estimated based on the profile likelihood method [38]. For 11 photons in the sidebands and 11 photons in the region where the signal is expected, the method estimates an upper bound of 9.6 photons per 100 s within the rocking curve width. This value accounts for an upper bound of the polarization purity of 8×10^{-11} (95% confidence level).

IV. SIGNIFICANCE FOR FUTURE EXPERIMENTS

Does this result enable, for example, the detection of vacuum birefringence? Considering the 300-TW laser available

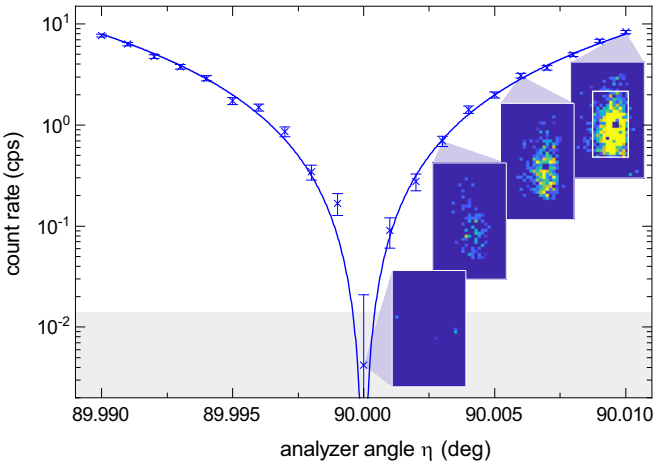

FIG. 3. Variation of the count rate close to the crossed polarizer setting. At exactly 90°, the count rate lies within the background noise (gray-shaded area). The values were obtained from the data of an energy- and space-resolving TIMEPIX detector. The corresponding intensity distributions are shown for specific positions at which in the upper one the white rectangle highlights the region of interest used for integration. The blue solid line describes the behavior of perfect polarizers. Error bars represent the statistical error.

at the HED beamline of the European XFEL (with pulses of 10 J and 30 fs) tightly focused to 2.5 μm, the ratio of the number of polarization flipped x rays after the interaction with the high-power laser to the number of incident x rays is 4×10^{-14} according to ref. [20]. Considering the 6×10^7 photons per pulse behind the polarizer and a FEL pulse length of 100 fs, one requires 6.5×10^9 laser pulses or, in other units, 41 yr to detect the polarization flipped photons above the background with a confidence of 5σ. However, by decreasing the absorption in air and using a seeded FEL beam with a narrow bandwidth, we expect a gain in flux behind the polarizer of more than three orders of magnitude to about 1.5×10^{11} photons per pulse. This will drastically decrease the required number of laser pulses to 2.5×10^6, which corresponds to only 6 days acquisition time. A further prerequisite for such an experiment, which is still under investigation, is a focusing scheme for the FEL beam, which allows to match the spot sizes of both lasers by simultaneously maintaining the high polarization purity.

V. CONCLUSION

In conclusion, we demonstrated an unprecedented polarization purity of better than 8×10^{-11} at the European XFEL, which amounts to a suppression of the entire photon flux of this highly brilliant source to the noise level. This is an important step for future polarimetric experiments at XFELs. On the one hand, the high sensitivity achieved is pivotal for testing fundamental physical phenomena, such as vacuum birefringence. On the other hand, the realized purity corresponds to a well-defined quantum state of the x-ray photons, which will open new opportunities for quantum optics at XFELs. A comparison of the result with previous measurements at synchrotrons [31,33] shows that the sensitivity of x-ray polarimeters depends significantly on the parameters of the source. Improving the flux before the analyzer by reducing the mismatch between the SASE bandwidth and the energy acceptance of the polarizers by a seeded XFEL will be an important next step for applications with perfectly polarized x rays.

ACKNOWLEDGMENTS

We acknowledge European XFEL in Schenefeld, Germany for provision of x-ray free-electron laser beam time at Scientific Instrument HED and would like to thank the instrument group and facility staff for their assistance. This work has been funded by the Deutsche Forschungsgemeinschaft (DFG) under Grants No. 416700351 and No. 416607684 within the Research Unit FOR2783/1 and by the Bundesministerium für Bildung und Forschung (BMBF) under Grant No. 05K16SJ2.

[1] Y. Han and G. Li, Coherent optical communication using polarization multiple-input-multiple-output, Opt. Express **13**, 7527 (2005).

[2] G. B. Xavier, G. Vilela de Faria, G. P. Temporão, and J. P. von der Weid, Full polarization control for fiber optical quantum communication systems using polarization encoding, Opt. Express **16**, 1867 (2008).

[3] H. G. Tompkins and E. A. Irene, *Handbook of Ellipsometry* (William Andrew, Norwich, NY, 2005).

[4] J. L. Deuzé, F. M. Bréon, C. Devaux, P. Goloub, M. Herman, B. Lafrance, F. Maignan, A. Marchand, F. Nadal, G. Perry, and D. Tanré, Remote sensing of aerosols over land surfaces from POLDER-ADEOS-1 polarized measurements, J. Geophys. Res.: Atmospheres **106**, 4913 (2001).

[5] C. H. Bennett, F. Bessette, G. Brassard, L. Salvail, and J. Smolin, Experimental quantum cryptography, J. Cryptology **5**, 3 (1992).

[6] T. Jennewein, C. Simon, G. Weihs, H. Weinfurter, and A. Zeilinger, Quantum Cryptography with Entangled Photons, Phys. Rev. Lett. **84**, 4729 (2000).

[7] C. Kurtsiefer, P. Zarda, M. Halder, H. Weinfurter, P. Gorman, P. Tapster, and J. Rarity, Quantum cryptography: A step towards global key distribution, Nature (London) **419**, 450 (2002).

[8] K.-J. Boller, A. Imamoğlu, and S. E. Harris, Observation of Electromagnetically Induced Transparency, Phys. Rev. Lett. **66**, 2593 (1991).

[9] G. van der Laan and A. I. Figueroa, X-ray magnetic circular dichroism-a versatile tool to study magnetism, Coordination Chem. Rev. **277**, 95 (2014).

[10] A. Ney, V. Ney, K. Ollefs, D. Schauries, F. Wilhelm, and A. Rogalev, X-ray linear dichroism: An element-selective spectroscopic probe for local structural properties and valence, J. Surfaces Interfaces Materials **2**, 14 (2014).

[11] K. P. Heeg, H.-C. Wille, K. Schlage, T. Guryeva, D. Schumacher, I. Uschmann, K. S. Schulze, B. Marx, T. Kämpfer, G. G. Paulus, R. Röhlsberger, and J. Evers, Vacuum-assisted Generation and Control of Atomic Coherences at X-Ray Energies, Phys. Rev. Lett. **111**, 073601 (2013).

[12] K. P. Heeg, J. Haber, D. Schumacher, L. Bocklage, H.-C. Wille, K. S. Schulze, R. Loetzsch, I. Uschmann, G. G. Paulus, R. Rüffer, R. Röhlsberger, and J. Evers, Tunable Subluminal Propagation of Narrow-Band X-Ray Pulses, Phys. Rev. Lett. **114**, 203601 (2015).

[13] J. Haber, K. S. Schulze, K. Schlage, R. Loetzsch, L. Bocklage, T. Gurieva, H. Bernhardt, H.-C. Wille, R. Rüffer, I. Uschmann *et al.*, Collective strong coupling of x-rays and nuclei in a nuclear optical lattice, Nat. Photonics **10**, 445 (2016).

[14] L. G. Huang, H.-P. Schlenvoigt, H. Takabe, and T. E. Cowan, Ionization and reflux dependence of magnetic instability generation and probing inside laser-irradiated solid thin foils, Phys. Plasmas **24**, 103115 (2017).

[15] J. S. Toll, The dispersion relation for light and its application to problems involving electron pairs, Ph.D. thesis, Princeton University, 1952.

[16] J. J. Klein and B. P. Nigam, Birefringence of the vacuum, Phys. Rev. **135**, B1279 (1964).

[17] T. Heinzl, B. Liesfeld, K.-U. Amthor, H. Schwoerer, R. Sauerbrey, and A. Wipf, On the observation of vacuum birefringence, Opt. Commun. **267**, 318 (2006).

[18] F. Karbstein, H. Gies, M. Reuter, and M. Zepf, Vacuum birefringence in strong inhomogeneous electromagnetic fields, Phys. Rev. D **92**, 071301(R) (2015).

[19] H.-P. Schlenvoigt, T. Heinzl, U. Schramm, T. E. Cowan, and R. Sauerbrey, Detecting vacuum birefringence with x-ray free electron lasers and high-power optical lasers: a feasibility study, Phys. Scr. **91**, 023010 (2016).

[20] F. Karbstein, Vacuum birefringence in the head-on collision of x-ray free-electron laser and optical high-intensity laser pulses, Phys. Rev. D **98**, 056010 (2018).

[21] W. Heisenberg and H. Euler, Folgerungen aus der Diracschen Theorie des Positrons, Z. Phys. **98**, 714 (1936).

[22] B. Shen, Z. Bu, J. Xu, T. Xu, L. Ji, R. Li, and Z. Xu, Exploring vacuum birefringence based on a 100 PW1, laser and an x-ray free electron laser beam, Plasma Phys. Controlled Fusion **60**, 044002 (2018).

[23] D. Xu, B. Shen, J. Xu, and Z. Liang, XFEL beamline design for vacuum birefringence experiment, Nucl. Instrum. Methods Phys. Res., Sect. A **982**, 164553 (2020).

[24] E. Alp, W. Sturhahn, and T. Toellner, Polarizer–analyzer optics, Hyperfine Interact. **125**, 45 (2000).

[25] M. Hart, X-ray polarization phenomena, Philos. Mag. Part B **38**, 41 (1978).

[26] M. Hart and A. R. D. Rodrigues, Tuneable polarizers for x-rays and neutrons, Philos. Mag. Part B **40**, 149 (1979).

[27] T. S. Toellner, E. E. Alp, W. Sturhahn, T. M. Mooney, X. Zhang, M. Ando, Y. Yoda, and S. Kikuta, Polarizer/analyzer filter for nuclear resonant scattering of synchrotron radiation, Appl. Phys. Lett. **67**, 1993 (1995).

[28] D. Siddons, J. Hastings, U. Bergmann, F. Sette, and M. Krisch, Mössbauer spectroscopy using synchrotron radiation: overcoming detector limitations, Nucl. Instrum. Methods Phys. Res., Sect. B **103**, 371 (1995).

[29] R. Röhlsberger, E. Gerdau, R. Rüffer, W. Sturhahn, T. S. Toellner, A. I. Chumakov, and E. E. Alp, X-ray optics for μeV-resolved spectroscopy, Nucl. Instrum. Methods Phys. Res., Sect. A **394**, 251 (1997).

[30] B. Marx, I. Uschmann, S. Höfer, R. Lötzsch, O. Wehrhan, E. Förster, M. Kaluza, T. Stöhlker, H. Gies, C. Detlefs *et al.*, Determination of high-purity polarization state of x-rays, Opt. Commun. **284**, 915 (2011).

[31] B. Marx, K. S. Schulze, I. Uschmann, T. Kämpfer, R. Lötzsch, O. Wehrhan, W. Wagner, C. Detlefs, T. Roth, J. Härtwig, E. Förster, T. Stöhlker, and G. G. Paulus, High-Precision X-Ray Polarimetry, Phys. Rev. Lett. **110**, 254801 (2013).

[32] K. S. Schulze, Fundamental limitations of the polarization purity of x rays, APL Photonics **3**, 126106 (2018).

[33] H. Bernhardt, A. T. Schmitt, B. Grabiger, B. Marx-Glowna, R. Loetzsch, H.-C. Wille, D. Bessas, A. I. Chumakov, R. Rüffer, R. Röhlsberger, T. Stöhlker, I. Uschmann, G. G. Paulus, and K. S. Schulze, Ultra-high precision x-ray polarimetry with artificial diamond channel cuts at the beam divergence limit, Phys. Rev. Research **2**, 023365 (2020).

[34] A. T. Schmitt, Y. Joly, K. S. Schulze, B. Marx-Glowna, I. Uschmann, B. Grabiger, H. Bernhardt, R. Loetzsch, A. Juhin, J. Debray, H.-C. Wille, H. Yavaş, G. G. Paulus, and R. Röhlsberger, Disentangling x-ray dichroism and birefringence via high-purity polarimetry, Optica **8**, 56 (2021).

[35] T. Tschentscher, C. Bressler, J. Grünert, A. Madsen, A. P. Mancuso, M. Meyer, A. Scherz, H. Sinn, and U. Zastrau, Photon beam transport and scientific instruments at the European XFEL, Appl. Sci. **7**, 592 (2017).

[36] W. L. Bond, Precision lattice constant determination, Acta Crystallogr. **13**, 814 (1960).

[37] X. Llopart, R. Ballabriga, M. Campbell, L. Tlustos, and W. Wong, Timepix, a 65k programmable pixel readout chip for arrival time, energy and/or photon counting measurements, Nucl. Instrum. Methods Phys. Res., Sect. A **581**, 485 (2007).

[38] W. A. Rolke and A. M. López, Confidence intervals and upper bounds for small signals in the presence of background noise, Nucl. Instrum. Methods Phys. Res., Sect. A **458**, 745 (2001).